PHYSICAL REVIEW B **96**, 035428 (2017)

Super-micron-scale atomistic simulation for electronic transport with atomic vibration: Unified approach from quantum to classical transport

Keisuke Ishizeki,[1] Kenji Sasaoka,[2,3] Satoru Konabe,[1,4] Satofumi Souma,[3] and Takahiro Yamamoto[1,4,5]

[1] *Department of Electrical Engineering, Tokyo University of Science, Tokyo 125-8585, Japan*
[2] *Organization of Advanced Science and Technology, Kobe University, Kobe 657-8501, Japan*
[3] *Department of Electrical and Electronic Engineering, Kobe University, Kobe 657-8501, Japan*
[4] *Research Institute for Science and Technology, Tokyo University of Science, Tokyo 125-8585, Japan*
[5] *Department of Liberal Arts (Physics), Tokyo University of Science, Tokyo 125-8585, Japan*

(Received 1 January 2017; revised manuscript received 3 April 2017; published 20 July 2017)

We develop a powerful simulation method that can treat electronic transport in a super-micron-scale open system with atomic vibration at finite temperature. As an application of the developed method to realistic materials, we simulate electronic transport in metallic single-walled carbon nanotubes from nanometer scale to micrometer scale at room temperature. Based on the simulation results, we successfully identify two different crossovers, namely, ballistic to diffusive crossover and coherent to incoherent crossover, simultaneously and with equal footing, from which the mean free path and the phase coherence length can be extracted clearly. Moreover, we clarify the scaling behavior of the electrical resistance and the electronic current in the crossover regime.

DOI: 10.1103/PhysRevB.96.035428

I. INTRODUCTION

Electronic transport properties depend on the system size especially for low-dimensional systems. When the system length L is much shorter (longer) than the mean free path L_{m}, transport occurs in a ballistic (diffusive) manner. For ballistic transport, the electrical resistance R is independent of L and is quantized with a universal value of $h/(2e^2M)$, where h is the Planck constant, e is the elementary charge, and M is an integer [1–3]. On the other hand, for diffusive transport, R is proportional to L, as described by Ohm's law. There is another way to characterize the transport behavior. When L is much shorter than the phase coherence length L_ϕ, the transport exhibits quantum interference effects, such as the Aharonov-Bohm effect [4] and Anderson localization [5]. Conversely, when $L \gg L_\phi$, the particle nature dominates, where interference effects do not occur. Thus far, transport properties have been studied based on different transport theories depending on the transport regime. Therefore, it is less clear how we treat and understand the intermediate regime between different transport regimes from the ballistic (coherent) transport to the diffusive (incoherent) transport.

Understanding the transport properties in the intermediate regime is very challenging from both scientific and engineering viewpoints. For example, a single-walled carbon nanotube (SWNT) is an ideal realistic material for investigating various aspects of electronic transport in a one-dimensional system, including the intermediate regime, because the length of an SWNT ranges from the nanometer scale to the micrometer scale. There are some numerical simulation methods for investigating the transport properties, for example, the nonequilibrium Green's function (NEGF) method [6–8], the Wigner Monte Carlo method [9–11], and the single-electron density matrix method [12]. However, such methods are practically difficult to calculate electronic transport properties for realistic system size although they are applicable to these phenomena in principle. Another practicable method available for such a purpose is the order-N calculation method developed by combining the wave packet diffusion (WPD) method with the molecular dynamics (MD) simulation, which can make the transport calculation for a huge system possible using the Kubo-Greenwood formula [13–15]. One drawback of the WPD method is that it cannot treat nonequilibrium transport at finite voltages among multiple reservoirs because this method is based on linear response theory with a single reservoir. Another drawback is that local physical quantities, such as the spatial distribution of electronic current, are difficult to be obtained in a straightforward manner. The time-dependent Schrödinger equation method for an open system [16–18] (hereinafter called open TDSE method) is the effective one that overcomes the above-mentioned drawbacks. In the present study, we thus develop a powerful simulation method by combining the open TDSE method with the MD simulation, which can seamlessly treat all transport regimes including intermediate regime, and elucidate the electronic transport of such a crossover regime in a large-scale open system.

II. MODEL AND SIMULATION METHOD

In the present study, we develop a powerful simulation method on super-micron-scale atomistic simulation for electronic transport with thermal atomic vibration by combining the open TDSE method [17,18] with the MD simulation. The open TDSE method can treat a system having over one million atoms within order-N simulation with a Hamiltonian represented by the localized basis such as the atomic orbital basis and the real space basis, can be applied to an open system, and can obtain local quantities of the wave function that give the spatial distribution of various physical quantities. The Hamiltonian is determined depending on the motions of atoms controlled by the MD simulation. As a result, the developed method can simulate the electronic transport in a large-scale open system with atomic vibration due to all lattice vibration modes, including the anharmonicity of the potential variation, without any additional numerical cost. Moreover, the method provides an intuitive understanding of the electrical resistance R similar to the Landauer-Büttiker/NEGF formalism. Using

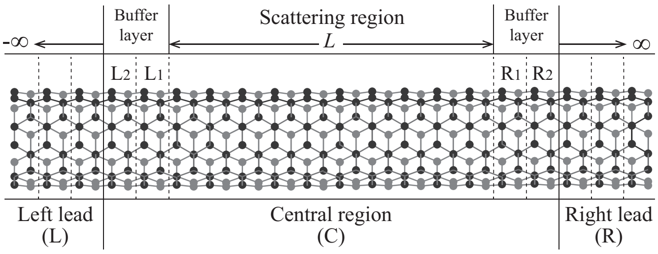

FIG. 1. Simulation model consists of three regions: the central region, the left lead, and the right lead. The central region is composed of a scattering region with atomic vibration and two buffer layers without vibration, each of which is composed of two unit cells. The central region is sandwiched between the two semi-infinite leads without atomic vibration.

this simulation method, we compute R for an individual armchair metallic SWNT within the wide band limit scheme.

A. Model

In this subsection, we provide the simulation model considered in the present study. As shown in Fig. 1, the simulation model consists of three regions: the central region (C), the left lead (L), and the right lead (R). The central region is composed of a scattering region including a finite-length SWNT with atomic vibration and two buffer layers, each of which includes two unit cells without atomic vibration. The buffer layers are set to calculate the current $j_{\epsilon,n}(t)$, as described later. The central region is sandwiched in between the left and the right leads, which are, respectively, composed of a semi-infinite SWNT without atomic vibration and assumed to connect to an electron reservoir that is always in thermal equilibrium. The Hamiltonian operator $\hat{H}(t)$ for the above-described system is obtained as

$$\hat{H}(t) = \hat{H}^{\mathrm{CC}}(t) + \sum_{\gamma=\mathrm{L,R}} (\hat{H}^{\gamma\gamma} + \hat{H}^{\mathrm{C}\gamma}), \tag{1}$$

where $\hat{H}^{\mathrm{CC}}(t)$ is the time-dependent Hamiltonian in the central region, $\hat{H}^{\gamma\gamma}$ is the time-independent Hamiltonian in the lead γ ($\gamma = \mathrm{L,R}$), and $\hat{H}^{\mathrm{C}\gamma}$ is the coupling Hamiltonian between the central region and the lead γ. In the present study, we use the π-orbital orthogonal tight-binding Hamiltonian. $\hat{H}^{\mathrm{CC}}(t)$ is obtained as

$$\hat{H}^{\mathrm{CC}}(t) = -\sum_{\langle i,j\rangle} \gamma_{ij}(t)\,|i\rangle\,\langle j| - \sum_{i} \epsilon_i\,|i\rangle\,\langle i|\,, \tag{2}$$

where $\langle i,j\rangle$ implies that the sum is taken only between nearest neighbor ith and jth carbon atoms, $\gamma_{ij}(t)$ is the corresponding hopping integral, and ϵ_i is the on-site energy on the ith carbon. $\gamma_{ij}(t)$ is obtained by the Harrison rule [22],

$$\gamma_{ij}(t) = \gamma_0 \frac{|\vec{R}_{0,i} - \vec{R}_{0,j}|^2}{|\vec{R}_i(t) - \vec{R}_j(t)|^2}, \tag{3}$$

where $\gamma_0 = 2.7$ eV, $\vec{R}_{0,i}$ is the position of the ith carbon in the optimized geometry, and $\vec{R}_i(t)$ is one at time t. $\vec{R}_i(t)$ is obtained from the classical MD simulation within the NTV ensemble [19] using the velocity scaling scheme [20,21], where thermal equilibrium is assumed. However, the atoms in the two buffer layers are fixed at the optimal positions because they do not vibrate. Therefore, $\hat{H}^{\mathrm{C}\gamma}$ and the hopping integral in the two buffer layers of $\hat{H}^{\mathrm{CC}}(t)$ do not depend on time. In the present study, we set ϵ_i to be 0 eV.

B. Simulation method

In this subsection, we explain the simulation method for the simulation model shown in Fig. 1. According to the Landauer-Büttiker formalism for steady-state transport, the electrical conductance in the low bias limit is expressed as

$$G(\epsilon_{\mathrm{F}}) = G_0 \int_{-\infty}^{\infty} \zeta(\epsilon)\left(-\frac{\partial f(\epsilon - \epsilon_{\mathrm{F}})}{\partial \epsilon}\right) d\epsilon, \tag{4}$$

where ϵ_{F} is the Fermi energy, $G_0 \equiv 2e^2/h$ is the quantum conductance, $f(\epsilon - \epsilon_{\mathrm{F}})$ is the Fermi distribution function, and $\zeta(\epsilon)$ is the effective transmission function including the phase-breaking effect due to the electron-phonon scattering [3] in the scattering region. The effective transmission function $\zeta(\epsilon)$ can be expressed from its definition as

$$\zeta(\epsilon) \equiv \sum_{n} \frac{j_{\epsilon,n}^{\mathrm{out}}}{j_{\epsilon,n}^{\mathrm{in}}}. \tag{5}$$

Here, $j_{\epsilon,n}^{\mathrm{in}}$ is the time-independent dimensionless current injected from the left lead with a certain energy ϵ and a band index n, $j_{\epsilon,n}^{\mathrm{out}}$ is the steady-state current defined as

$$j_{\epsilon,n}^{\mathrm{out}} = \lim_{t\to\infty} \frac{1}{t - t_0} \int_{t_0}^{t} j_{\epsilon,n}(t')dt', \tag{6}$$

and t_0 is a certain time in a steady state. In Eq. (6), $j_{\epsilon,n}(t)$, defined by Eq. (16) below, is the time-dependent dimensionless current flowing from the layer R_1 to the layer R_2 with ϵ and n (see Fig. 1 from the definitions of R_1 and R_2). When $j_{\epsilon,n}^{\mathrm{out}}$ and $j_{\epsilon,n}^{\mathrm{in}}$ are always constant to $j_{\epsilon_{\mathrm{F}},n}^{\mathrm{out}}$ and $j_{\epsilon_{\mathrm{F}},n}^{\mathrm{in}}$ around ϵ_{F}, which is valid for a metallic SWNT at room temperature due to the linear dispersion, Eq. (4) becomes

$$G(\epsilon_{\mathrm{F}}) = G_0 \zeta(\epsilon_{\mathrm{F}}). \tag{7}$$

To obtain $j_{\epsilon_{\mathrm{F}},n}(t)$, we solve the Schrödinger equation for an open system with the tight-binding Hamiltonian. Within the central region, the time evolution of the wave function vector $\vec{\Psi}_{\pm,\epsilon_{\mathrm{F}},n}^{\mathrm{C}}(t)$ with ϵ_{F} and n is described by

$$i\hbar \frac{\partial \vec{\Psi}_{\pm,\epsilon_{\mathrm{F}},n}^{\mathrm{C}}(t)}{\partial t} = H^{\mathrm{CC}}(t)\vec{\Psi}_{\pm,\epsilon_{\mathrm{F}},n}^{\mathrm{C}}(t) + \vec{S}_{\pm,\epsilon_{\mathrm{F}},n}^{\gamma}(t) + \vec{D}_{\pm,\epsilon_{\mathrm{F}},n}(t), \tag{8}$$

where $\hbar \equiv h/2\pi$ is the Dirac constant, $H^{\mathrm{CC}}(t)$ is the Hamiltonian matrix with the atomic orbital basis, and the subscript of $+(-)$ indicates the right-going (left-going) state. $\vec{S}_{\pm,\epsilon_{\mathrm{F}},n}^{\gamma}(t)$ represents influx of electrons from the lead γ, and is given by

$$\vec{S}_{\pm,\epsilon_{\mathrm{F}},n}^{\gamma}(t) = H^{\mathrm{C}\gamma} \frac{\vec{\phi}_{\pm,\epsilon_{\mathrm{F}},n}^{\gamma}}{\sqrt{v_n}} \exp\left(-i\frac{\epsilon_{\mathrm{F}}}{\hbar}t\right). \tag{9}$$

Here, $\vec{\phi}_{\pm,\epsilon_{\mathrm{F}},n}^{\gamma}$ is the wave function vector in the isolated lead γ normalized by the number of atoms in a unit cell, and v_n is the group velocity of $\vec{\phi}_{\pm,\epsilon_{\mathrm{F}},n}^{\gamma}$ toward the central region, which is introduced to make $j_{\epsilon_{\mathrm{F}},n}(t)$ dimensionless [3]. $\vec{D}_{\pm,\epsilon_{\mathrm{F}},n}(t)$

represents outflux of electrons from the central region into the two leads. $\vec{D}_{\pm,\epsilon_{\mathrm{F}},n}(t)$ is given by

$$\vec{D}_{\pm,\epsilon_{\mathrm{F}},n}(t) = (\Sigma^{\mathrm{L}}(\epsilon_{\mathrm{F}}) + \Sigma^{\mathrm{R}}(\epsilon_{\mathrm{F}}))\vec{\Psi}^{\mathrm{C}}_{\pm,\epsilon_{\mathrm{F}},n}(t), \tag{10}$$

using the retarded self-energy $\Sigma^{\gamma}(\epsilon_{\mathrm{F}})$ due to the lead γ within the wide band limit scheme. Details of derivation of Eqs. (8)–(10) are provided in Appendix A. Here, the point is that $\vec{\phi}^{\gamma}_{\pm,\epsilon_{\mathrm{F}},n}$ and $\Sigma^{\gamma}(\epsilon_{\mathrm{F}})$ can be calculated using the mode matching method enabling one to treat the realistic structure like an SWNT [23,24].

As an initial state required in the time-evolution simulation based on Eq. (8), we choose the wave function in a steady state for the time-independent optimized system [25]. In this simulation, Eq. (8) is discretized based on the finite difference scheme:

$$\bar{U}(t)\vec{\Psi}^{\mathrm{C}}_{\pm,\epsilon_{\mathrm{F}},n}(t+\Delta t) = U(t)\vec{\Psi}^{\mathrm{C}}_{\pm,\epsilon_{\mathrm{F}},n}(t) + \vec{s}^{\,\gamma}_{\pm,\epsilon_{\mathrm{F}},n}(t), \tag{11}$$

where Δt is the time spacing. $\bar{U}(t)$ and $U(t)$ are, respectively, given as

$$\bar{U}(t) = I + \frac{i\Delta t}{2\hbar}H_{\mathrm{eff}}(t+\Delta t), \tag{12}$$

and

$$U(t) = I - \frac{i\Delta t}{2\hbar}H_{\mathrm{eff}}(t). \tag{13}$$

Here, I is the unit matrix, and the effective Hamiltonian matrix $H_{\mathrm{eff}}(t)$ is defined as

$$H_{\mathrm{eff}}(t) \equiv H^{\mathrm{CC}}(t) + \Sigma^{\mathrm{L}}(\epsilon_{\mathrm{F}}) + \Sigma^{\mathrm{R}}(\epsilon_{\mathrm{F}}). \tag{14}$$

$\vec{s}^{\,\gamma}_{\pm,\epsilon_{\mathrm{F}},n}(t)$ is represented by

$$\vec{s}^{\,\gamma}_{\pm,\epsilon_{\mathrm{F}},n}(t) = -\frac{i\Delta t}{2\hbar}\big(\vec{S}^{\gamma}_{\pm,\epsilon_{\mathrm{F}},n}(t) + \vec{S}^{\gamma}_{\pm,\epsilon_{\mathrm{F}},n}(t+\Delta t)\big). \tag{15}$$

In the absence of the influx and the outflux terms, Eq. (11) reduces to Cayley's form for wave packet propagation in a closed system [26], meaning that Eq. (11) is Cayley's form generalized for an open system.

From $\vec{\Psi}^{\mathrm{C}}_{+,\epsilon_{\mathrm{F}},n}(t)$, we can calculate the dimensionless current $j_{\epsilon_{\mathrm{F}},n}(t)$ using the following relationship:

$$j_{\epsilon_{\mathrm{F}},n}(t) = \frac{2a}{\hbar}\mathrm{Im}\big[\big(\vec{\Psi}^{\mathrm{R}_2}_{+,\epsilon_{\mathrm{F}},n}(t)\big)^{\dagger}H^{\mathrm{R}_2,\mathrm{R}_1}\vec{\Psi}^{\mathrm{R}_1}_{+,\epsilon_{\mathrm{F}},n}(t)\big], \tag{16}$$

where a is the length of a unit cell, $\vec{\Psi}^{\mathrm{R}_{1(2)}}_{+,\epsilon_{\mathrm{F}},n}(t)$ is the wave function vector in the layer $\mathrm{R}_1(\mathrm{R}_2)$, and $H^{\mathrm{R}_1,\mathrm{R}_2}$ is the Hamiltonian matrix connecting R_1 and R_2.

We present our calculation results for the electronic transport properties in an individual armchair SWNT, characterized by the chiral index (m,m) with $4m$ carbon atoms in a unit cell [27,28]. In the present study, we use a pristine SWNT, i.e., without any vacancies or defects, as a model system to focus on the effect of electron-phonon scattering. We treat the phonons by the classical MD simulation, where the occupation for phonons with high energy is overestimated in general. However, in the low bias limit at room temperature as considered in the present study, the electron-phonon scattering is mainly dominated by acoustic phonons [29,30], meaning that the occupation of high frequency phonons is not an influential factor and thus the use of the classical MD simulation can be effectively justified. We use the optimized Tersoff potential [31] for C-C bonds, which reproduces the phonon dispersion of an SWNT very well, in the constant temperature MD simulation, where $\Delta t = 0.1$ fs is the time spacing in Eq. (11), and $\epsilon_{\mathrm{F}} = 0$ eV in Eq. (16). The initial state at $t = 0$ is the steady state that the current flows without atomic vibration [25]. We start the atomic vibration from $t = 0$.

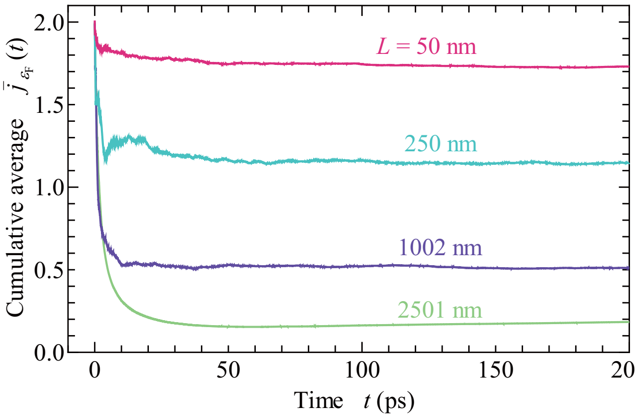

FIG. 2. Time t dependence of the cumulative average $\bar{j}_{\epsilon_{\mathrm{F}}}(t)$ at 300 K for a (5,5)-SWNT from 0 to 200 ps. $\bar{j}_{\epsilon_{\mathrm{F}}}(t)$ arrives at a steady current as $t \to \infty$ for every L.

III. RESULTS AND DISCUSSION

A. Time-dependent current

In this subsection, we discuss the time-dependent current. Figure 2 shows the time t dependence of the cumulative average defined as

$$\bar{j}_{\epsilon_{\mathrm{F}}}(t) \equiv \frac{1}{t}\sum_{n}\int_{0}^{t} j_{\epsilon_{\mathrm{F}},n}(t')dt', \tag{17}$$

for a (5,5)-SWNT with a system length L of 50 to 2501 nm (200 to 10 000 unit cells) from 0 to 200 ps. As shown in Fig. 2, $\bar{j}_{\epsilon_{\mathrm{F}}}(t)$ decreases rapidly as t varies from 0 to 10 ps, and finally becomes constant for specific values of L, indicating the establishment of a certain steady state. The constant value of $\bar{j}_{\epsilon_{\mathrm{F}}}(t)$ becomes smaller as L increases because electrons suffer from the electron-phonon scattering more significantly. Note that while these converged current values are evaluated for electrons injected from the left lead, ones for electrons injected from the right lead exhibit similar behavior. We regard $j_{\epsilon_{\mathrm{F}},n}(t)$ from 160 to 200 ps as the steady-state current and calculate $R = G^{-1}$ based on Eq. (7).

B. Electrical resistance and mean free path

Figure 3 shows the system length L dependence of R of an armchair SWNT for four different diameters d_t at 300 K with lengths ranging from 2.5 to 3000 nm (10–12 000 unit cells). This figure clearly shows that the transport regime seamlessly changes from ballistic to diffusive transport. In the limit $L/L_{\mathrm{m}} \to 0$, R reaches half the quantum resistance $(R_0/2)$ because the number of conduction channels is 2 regardless of L, where L_{m} is the mean free path. On the other hand, in the limit $L/L_{\mathrm{m}} \to \infty$, R is proportional to L. In the following,

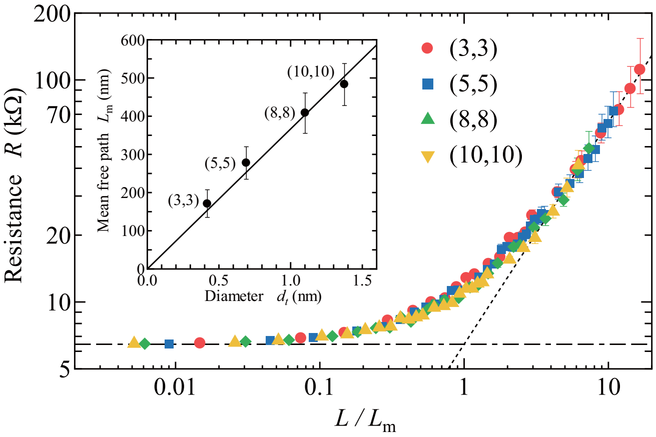

FIG. 3. System length L dependence of the electrical resistance R of an armchair SWNT at 300 K. The error bars originate from the standard error of $j_{\epsilon_\mathrm{F},n}(t)$ from 160 to 200 ps per 1 ps. The dotted line represents $R = (R_0/2)L/L_\mathrm{m}$ in the diffusive limit at $L/L_\mathrm{m} \to \infty$, where L_m is the mean free path, and the dash-dotted line represents $R = R_0/2$ in the ballistic limit at $L/L_\mathrm{m} \to 0$. The inset shows that the diameter d_t dependence of L_m at 300 K as $L_\mathrm{m} = 366.6d_t$. The error bars originate from those of R.

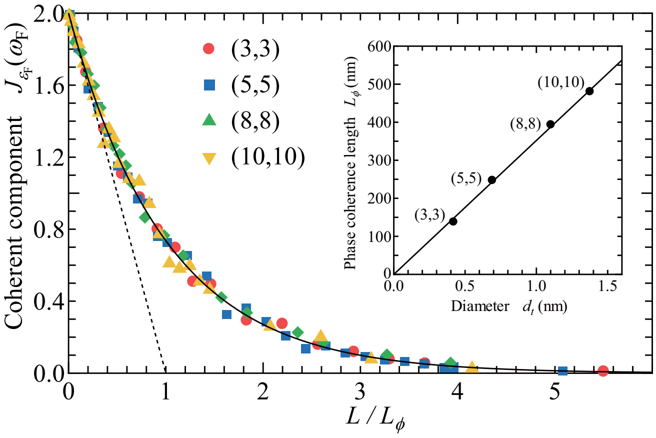

FIG. 4. System length L dependence of the coherent component $J_{\epsilon_\mathrm{F}}(\omega_\mathrm{F})$ for an armchair SWNT at 300 K. $J_{\epsilon_\mathrm{F}}(\omega_\mathrm{F})$ behaves as $J_{\epsilon_\mathrm{F}}(\omega_\mathrm{F}) = 2\exp(-L/L_\phi)$ (solid line), where L_ϕ is the phase coherence length. The dotted line, $1 - L/L_\phi$, shows the asymptotic behavior of $J_{\epsilon_\mathrm{F}}(\omega_\mathrm{F})$ for $L/L_\phi \to 0$. The inset shows the diameter d_t dependence of L_ϕ at 300 K as $L_\phi = 352.1d_t$.

let us discuss the transport properties in the diffusive and the ballistic regimes in detail. The L dependence of R in the diffusive regime is described by

$$R = \frac{R_0}{M}\frac{L}{L_\mathrm{m}} \quad (L/L_\mathrm{m} \gg 1), \tag{18}$$

where $R_0 = G_0^{-1}$ is the quantum resistance and M is the number of conduction channels [3] ($M = 2$ for an armchair SWNT at ϵ_F). Comparing Eq. (18) with the simulation results shown in Fig. 3, we can estimate L_m for an SWNT with diameters d_t as shown in Appendix B. Knowing the value of L_m, we can identify the following two distinct transport regimes. For $L/L_\mathrm{m} \gg 1$, R shows Ohm's law as described by Eq. (18) (the dotted line in Fig. 3). On the other hand, for $L/L_\mathrm{m} \ll 1$, R is equivalent to $R_0/2$ (the dash-dotted line in Fig. 3) characterizing the ballistic transport. We then consider the intermediate regime around $L/L_\mathrm{m} \sim 1$ between the ballistic and the diffusive transport regimes, referred to as the quasiballistic transport regime. Interestingly, even in the quasiballistic regime, R with various d_t can be expressed by a single curve with respect to L/L_m. Thus, we found that R for an armchair SWNT in the entire regime from ballistic to diffusive transport regimes follows the scaling law $R = f(L/L_\mathrm{m})$.

The inset in Fig. 3 shows the d_t dependence of L_m for (3,3), (5,5), (8,8), and (10,10)-SWNTs at 300 K, which shows that L_m increases linearly with d_t, where $L_\mathrm{m} = 366.6d_t$. This d_t dependence of R has been discussed by other theoretical and numerical methods [15,33]. Such behavior originates from the fact that the relaxation time derived from Fermi's golden rule is proportional to d_t, because the density of states in the final states backscattered by acoustic phonons from an initial state is inversely proportional to d_t [32–34]. Based on these relationships between d_t and L_m and between L/L_m and R, we can estimate R even in the intermediate regime of arbitrary d_t.

C. Decoherence and phase relaxation length

We then estimate the phase coherence length L_ϕ that determines the crossover from coherent to incoherent transport. To estimate L_ϕ, we extract the coherent component of the current from the total electronic current in the following manner. Applying a Fourier transform to the wave function,

$$\vec{\Psi}^{\mathrm{R}_{1(2)}}_{+,\epsilon_\mathrm{F},n}(t') = \sqrt{\frac{t-t_0}{2\pi}}\int_{-\infty}^{\infty}\exp(-i\omega t')\vec{\Phi}^{\mathrm{R}_{1(2)}}_{+,\epsilon_\mathrm{F},n}(\omega)d\omega. \tag{19}$$

Equation (6) for ϵ_F can be rewritten as

$$j^{\mathrm{out}}_{\epsilon_\mathrm{F},n} = \int_{-\infty}^{\infty} J_{\epsilon_\mathrm{F},n}(\omega)d\omega, \tag{20}$$

$$J_{\epsilon_\mathrm{F},n}(\omega) \equiv \frac{2a}{\hbar}\mathrm{Im}\left[\left(\vec{\Phi}^{\mathrm{R}_2}_{+,\epsilon_\mathrm{F},n}(\omega)\right)^{\dagger} H^{\mathrm{R}_2,\mathrm{R}_1}\vec{\Phi}^{\mathrm{R}_1}_{+,\epsilon_\mathrm{F},n}(\omega)\right], \tag{21}$$

where ω is the angular frequency. We now focus on the component of $J_{\epsilon_\mathrm{F}}(\omega_\mathrm{F})$ defined as

$$J_{\epsilon_\mathrm{F}}(\omega_\mathrm{F}) \equiv \sum_n J_{\epsilon_\mathrm{F},n}(\omega_\mathrm{F}), \tag{22}$$

with $\omega_\mathrm{F} = \epsilon_\mathrm{F}/\hbar$. $J_{\epsilon_\mathrm{F}}(\omega_\mathrm{F})$ is the coherent component preserving ϵ_F of an incident electron from the left lead to the central region. Figure 4 shows L dependence of $J_{\epsilon_\mathrm{F}}(\omega_\mathrm{F})$ flowing through an armchair SWNT for four different diameters at 300 K with lengths ranging from 2.5 to 3000 nm. We can see that $J_{\epsilon_\mathrm{F}}(\omega_\mathrm{F})$ decreases exponentially with increasing L.

Next, we explain how to extract L_ϕ from $J_{\epsilon_\mathrm{F}}(\omega_\mathrm{F})$. In the presence of atomic vibration, the current amplitude for the coherent component is known to decay as $\exp(-t/\tau_\phi)$ with time t, where τ_ϕ is the phase-relaxation time [3]. Electrons with ϵ_F propagate ballistically, preserving the Fermi velocity v_F through a distance shorter than $L_\mathrm{m} = v_\mathrm{F}\tau_\mathrm{m}$, where τ_m is the momentum relaxation time. Thus, when $\tau_\phi < \tau_\mathrm{m}$, L_ϕ can be written as $L_\phi = v_\mathrm{F}\tau_\phi$. Consequently, the current amplitude for the coherent component decreases by a factor of $\exp(-L/L_\phi)$

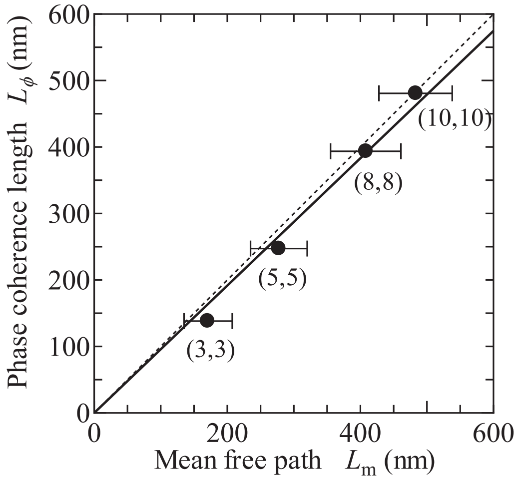

FIG. 5. Relationship between the mean free path $L_{\rm m}$ and the phase coherence length L_ϕ for an armchair SWNT at 300 K. The solid line, shown as $L_\phi = 0.958 L_{\rm m}$, is always under the dotted line shown as $L_\phi = L_{\rm m}$. This means that $L_{\rm m}$ is always longer than L_ϕ.

when $L_\phi < L_{\rm m}$. In fact, we can fit the simulation data using a universal function,

$$J_{\epsilon_{\rm F}}(\omega_{\rm F}) = M \exp\left(-\frac{L}{L_\phi}\right), \tag{23}$$

where M is the number of conduction channels. Using Eq. (23), we can estimate L_ϕ as shown in Appendix C. This means that the assumption of $L_\phi < L_{\rm m}$ is indeed satisfied. This originated with the suppression of backscattering, which is a specific feature of an SWNT [33]. Note that this method to extract L_ϕ can be also applied beyond the wide band limit scheme.

The inset of Fig. 4 shows the d_t dependence of L_ϕ for (3,3), (5,5), (8,8), and (10,10)-SWNTs at 300 K. Similar to the argument of $L_{\rm m}$, we can see that L_ϕ increases linearly with d_t as $L_\phi = 352.1 d_t$. In the following, we explain the origin of $L_\phi \propto d_t$. From the insets of Figs. 3 and 4, we found that $L_\phi < L_{\rm m}$ and, consequently, verified that $L_\phi = v_{\rm F}\tau_\phi$. On the other hand, $\tau_{\rm m}^{-1}$ and τ_ϕ^{-1} can be written as $\tau_{\rm m}^{-1} = \alpha_{\rm m}\tau_{\rm c}^{-1}$ and $\tau_\phi^{-1} = \alpha_\phi \tau_{\rm c}^{-1}$, respectively, where $\tau_{\rm c}$ is the time for an individual collision, and $\alpha_{\rm m}$ (α_ϕ) is the effective factor for momentum (phase) relaxation [3]. We thus obtain the relationship $L_\phi / L_{\rm m} = \alpha_{\rm m}/\alpha_\phi \equiv \alpha$, where α is constant with respect to d_t, and our simulation yields $\alpha = 0.958$ as shown in Fig. 5. From this result and $L_{\rm m} \propto d_t$ as discussed in the argument about $L_{\rm m}$, we obtain the relationship of $L_\phi \propto d_t$.

IV. SUMMARY

In summary, we developed a powerful simulation method that can treat electronic transport in a super-micron-scale open system with atomic vibration at finite temperature, and investigated the system length dependence of the electrical resistance of an armchair metallic SWNT from a few nanometers to a few micrometers. Our results seamlessly described the crossover behavior of the electronic transport both from the ballistic regime to the diffusive regime and from the coherent regime to the incoherent regime. Based on these results, we obtained the mean free path and the phase coherence length, both of which exhibited a linear dependence on the diameter of a metallic SWNT. The scaling behavior of the electronic transport was also discussed. These results are not only crucial to understanding the entire regime of electronic transport, but also useful for simulating future electronic devices of an SWNT, the lengths of which are within the crossover regime.

ACKNOWLEDGMENT

This work was supported, in part, by JSPS KAKENHI Grant No. 15H03523.

APPENDIX A: DERIVATION OF THE TIME-DEPENDENT SCHRÖDINGER EQUATION FOR AN OPEN SYSTEM

In the following, we derive the time-dependent Schrödinger equation for an open system as shown in Eq. (8). The Hamiltonian matrix with the atomic orbital basis for the system shown in Fig. 1 is decomposed into nine block matrices as

$$H(t) = \begin{pmatrix} H^{\rm LL} & H^{\rm LC} & 0 \\ H^{\rm CL} & H^{\rm CC}(t) & H^{\rm CR} \\ 0 & H^{\rm RC} & H^{\rm RR} \end{pmatrix}, \tag{A1}$$

where $H^{\alpha\alpha}$ and $H^{\alpha\beta}$ ($\alpha,\beta = {\rm L, C, R}$ and $\alpha \neq \beta$) are, respectively, a diagonal and an off-diagonal part of the Hamiltonian matrix. In this simulation, we define the diagonal block in Eq. (A1),

$$H(t) = \begin{pmatrix} H^{\rm LL} & 0 & 0 \\ 0 & H^{\rm CC}(t) & 0 \\ 0 & 0 & H^{\rm RR} \end{pmatrix}, \tag{A2}$$

as the unperturbed Hamiltonian matrix, and define the off-diagonal block in Eq. (A1),

$$H' = \begin{pmatrix} 0 & H^{\rm LC} & 0 \\ H^{\rm CL} & 0 & H^{\rm CR} \\ 0 & H^{\rm RC} & 0 \end{pmatrix}, \tag{A3}$$

as the perturbed Hamiltonian matrix.

Here, we introduce the Lippmann-Schwinger equation for the system shown in Fig. 1, which is given as

$$\vec{\Psi}(t) = \vec{\psi}(t) + \int_{-\infty}^{\infty} G(t,t') H' \vec{\psi}(t') dt', \tag{A4}$$

where $G(t,t')$ is the matrix representation of the retarded Green's function. $\vec{\Psi}(t)$ and $\vec{\psi}(t)$, respectively, denote the vector describing the states for the whole system and the unperturbed states.

The Green's function matrix can be decomposed as well as the Hamiltonian matrix shown in Eq. (A1) as

$$G(t,t') = \begin{pmatrix} G^{\rm LL}(t,t') & G^{\rm LC}(t,t') & G^{\rm LR}(t,t') \\ G^{\rm CL}(t,t') & G^{\rm CC}(t,t') & G^{\rm CR}(t,t') \\ G^{\rm RL}(t,t') & G^{\rm RC}(t,t') & G^{\rm RR}(t,t') \end{pmatrix}, \tag{A5}$$

where the superscript has the same meaning as Eq. (A1). $\vec{\Psi}(t)$ and $\vec{\psi}(t)$ can be also represented as

$$\vec{\Psi}(t)=\begin{pmatrix}\vec{\Psi}^{\rm L}(t)\\ \vec{\Psi}^{\rm C}(t)\\ \vec{\Psi}^{\rm R}(t)\end{pmatrix}, \tag{A6}$$

$$\vec{\psi}(t)=\begin{pmatrix}\vec{\psi}^{\rm L}(t)\\ \vec{\psi}^{\rm C}(t)\\ \vec{\psi}^{\rm R}(t)\end{pmatrix}. \tag{A7}$$

$\vec{\Psi}^\alpha(t)$ and $\vec{\psi}^\alpha(t)$ ($\alpha = $ L, C, R), respectively, consist of the perturbed and unperturbed wave functions positioned in the region α. By substituting Eqs. (A3), (A5), (A6), and (A7) into the Lippmann-Schwinger equation (A4), we obtain the equation,

$$\vec{\Psi}^\alpha(t)=\vec{\psi}^\alpha(t)+\sum_{\gamma={\rm L,R}}\int_{-\infty}^{\infty}G^{\alpha{\rm C}}(t,t_1)H^{{\rm C}\gamma}\vec{\psi}^{\gamma}(t_1)dt_1 + \sum_{\gamma={\rm L,R}}\int_{-\infty}^{\infty}G^{\alpha\gamma}(t,t_1)H^{\gamma{\rm C}}\vec{\psi}^{\rm C}(t_1)dt_1, \tag{A8}$$

where γ means the lead region ($\gamma = $ L,R).

The Green's function matrix for the whole system satisfies the equation,

$$i\hbar\frac{\partial G(t,t')}{\partial t}-H(t)G(t,t')=I\delta(t-t'), \tag{A9}$$

where $\delta(t-t')$ is the Dirac's delta function and I is the identity matrix. Using Eqs. (A1) and (A5), the LC- and RC-block components of Eq. (A9) are given as

$$i\hbar\frac{\partial G^{\gamma{\rm C}}(t,t')}{\partial t}-H^{\gamma\gamma}G^{\gamma{\rm C}}(t,t')-H^{\gamma{\rm C}}G^{\rm CC}(t,t')=0. \tag{A10}$$

To integrate the differential equation of Eq. (A10), we introduce the unperturbed retarded Green's function matrix $g^{\gamma\gamma}(t,t')$, which satisfies the equation,

$$-i\hbar\frac{\partial g^{\gamma\gamma}(t,t')}{\partial t}-g^{\gamma\gamma}(t,t')H^{\gamma\gamma}(t')=I^{\gamma\gamma}\delta(t-t'). \tag{A11}$$

The integration of Eq. (A10) gives the expression of $G^{\gamma{\rm C}}(t,t')$ in terms of the unperturbed Green's function,

$$G^{\gamma{\rm C}}(t,t')=\int_{-\infty}^{\infty}g^{\gamma\gamma}(t,t_1)H^{\gamma{\rm C}}G^{\rm CC}(t_1,t')dt_1. \tag{A12}$$

Here, note that the block component of $G^{\gamma{\rm C}}(t,t')$ is expressed only by $G^{\rm CC}(t,t')$ among the perturbed Green's function block matrices.

By substituting the equation of Eq. (A12) into Eq. (A9), we obtain the equation,

$$i\hbar\frac{\partial G^{\rm CC}(t,t')}{\partial t}-H^{\rm CC}(t)G^{\rm CC}(t,t') -\int_{-\infty}^{\infty}(\Sigma^{\rm L}(t,t_1)+\Sigma^{\rm R}(t,t_1))G^{\rm CC}(t_1,t')dt_1 = I^{\rm CC}\delta(t-t'). \tag{A13}$$

The self-energy $\Sigma^\gamma(t,t')$ due to the lead γ is defined by the equation,

$$\Sigma^\gamma(t,t')\equiv H^{{\rm C}\gamma}g^{\gamma\gamma}(t,t')H^{\gamma{\rm C}}. \tag{A14}$$

Next, for applying the open system equation of Eq. (A13) to quantum transport phenomena, we impose the additional condition for the unperturbed state $\vec{\psi}(t)$. The theoretical description of the nonequilibrium state in a mesoscopic system demands the scattering states coming from the lead L and the lead R, which, respectively, correspond to a right-going state and a left-going state. In this time, the unperturbed state is labeled by the incident energy ϵ and the band index n. In this simulation, for the right-going states from the lead L, the wave functions shown in Eqs. (A6) and (A7) are replaced by

$$\vec{\Psi}_{+,\epsilon,n}(t)=\begin{pmatrix}\vec{\Psi}^{\rm L}_{+,\epsilon,n}(t)\\ \vec{\Psi}^{\rm C}_{+,\epsilon,n}(t)\\ \vec{\Psi}^{\rm R}_{+,\epsilon,n}(t)\end{pmatrix}, \tag{A15}$$

$$\vec{\psi}_{+,\epsilon,n}(t)=\begin{pmatrix}\vec{\psi}^{\rm L}_{+,\epsilon,n}(t)\\ 0\\ 0\end{pmatrix}, \tag{A16}$$

where the subscript of $+$ indicates the right-going state. The substitution of Eqs. (A15) and (A16) into Eq. (A8) leads to

$$i\hbar\frac{\partial\vec{\Psi}^{\rm C}_{+,\epsilon,n}(t)}{\partial t}-H^{\rm CC}(t)\vec{\Psi}^{\rm C}_{+,\epsilon,n}(t) =\int_{-\infty}^{\infty}(\Sigma^{\rm L}(t,t_1)+\Sigma^{\rm R}(t,t_1))\vec{\Psi}^{\rm C}_{+,\epsilon,n}(t_1)dt_1+H^{\rm CL}\vec{\psi}^{\rm L}_{+,\epsilon,n}(t). \tag{A17}$$

In the same way for the left-going state from the lead R, we establish the perturbed and unperturbed wave functions as

$$\vec{\Psi}_{-,\epsilon,n}(t)=\begin{pmatrix}\vec{\Psi}^{\rm L}_{-,\epsilon,n}(t)\\ \vec{\Psi}^{\rm C}_{-,\epsilon,n}(t)\\ \vec{\Psi}^{\rm R}_{-,\epsilon,n}(t)\end{pmatrix}, \tag{A18}$$

$$\vec{\psi}_{-,\epsilon,n}(t)=\begin{pmatrix}0\\ 0\\ \vec{\psi}^{\rm R}_{-,\epsilon,n}(t)\end{pmatrix}, \tag{A19}$$

and replace Eq. (A8) by

$$i\hbar\frac{\partial\vec{\Psi}^{\rm C}_{-,\epsilon,n}(t)}{\partial t}-H^{\rm CC}(t)\vec{\Psi}^{\rm C}_{-,\epsilon,n}(t) =\int_{-\infty}^{\infty}(\Sigma^{\rm L}(t,t_1)+\Sigma^{\rm R}(t,t_1))\vec{\Psi}^{\rm C}_{-,\epsilon,n}(t_1)dt_1+H^{\rm CR}\vec{\psi}^{\rm R}_{-,\epsilon,n}(t). \tag{A20}$$

The subscript of $-$ indicates the left-going state.

Here, $\vec{\psi}^{\rm L}_{+,\epsilon,n}(t)$ and $\vec{\psi}^{\rm R}_{-,\epsilon,n}(t)$ are, respectively, replaced by $(\vec{\phi}^{\rm L}_{+,\epsilon,n}/\sqrt{v_n})\exp(-i\epsilon t/\hbar)$ and $(\vec{\phi}^{\rm R}_{-,\epsilon,n}/\sqrt{v_n})\exp(-i\epsilon t/\hbar)$. Moreover, by defining

$$\vec{S}^{\gamma}_{\pm,\epsilon,n}(t)\equiv H^{{\rm C}\gamma}\frac{\vec{\phi}^{\gamma}_{\pm,\epsilon,n}}{\sqrt{v_n}}\exp\left(-i\frac{\epsilon}{\hbar}t\right), \tag{A21}$$

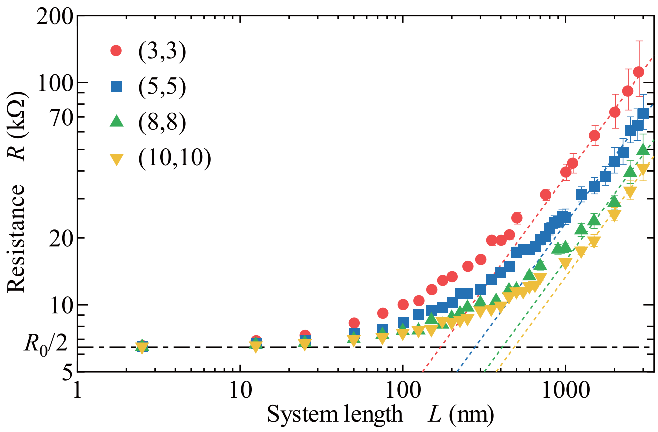

FIG. 6. System length L dependence of the electrical resistance R for an SWNT with various diameters at 300 K. The error bars originate from the standard error of $j_{\epsilon_F,n}(t)$ from 160 to 200 ps in the steady state per 1 ps. The dotted lines represent the resistance $R = (R_0/2)L/L_m$ in the diffusive limit $L \gg L_m$, and the dash-dotted line represents the resistance $R = R_0/2$ in the ballistic limit $L_m \gg L$.

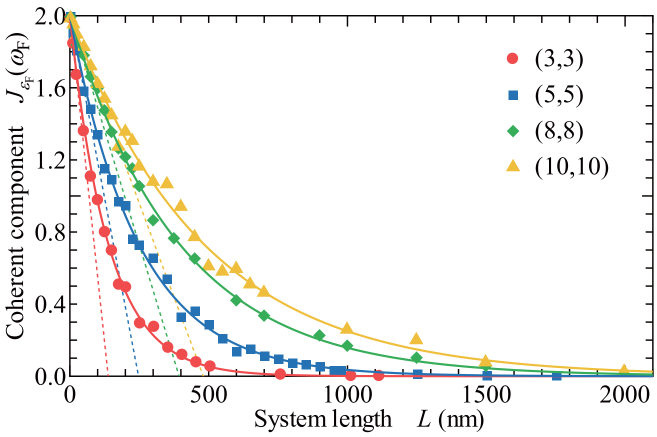

FIG. 7. System length L dependence of the coherent component $J_{\epsilon_F}(\omega_F)$ for an armchair SWNT with various diameters d_t at 300 K. The dotted lines, $1 - L/L_\phi$, show the asymptotic behavior of $J_{\epsilon_F}(\omega_F)$ for $L \to 0$.

and

$$\vec{D}_{\pm,\epsilon,n}(t) \equiv \int_{-\infty}^{\infty} (\Sigma^{L}(t,t_1) + \Sigma^{R}(t,t_1))\vec{\Psi}^{C}_{\pm,\epsilon,n}(t_1)dt_1, \quad \text{(A22)}$$

Eqs. (A17) and (A20) become

$$i\hbar\frac{\partial \vec{\Psi}^{C}_{\pm,\epsilon,n}(t)}{\partial t} = H^{CC}(t)\vec{\Psi}^{C}_{\pm,\epsilon,n}(t) + \vec{S}^{\gamma}_{\pm,\epsilon,n}(t) + \vec{D}_{\pm,\epsilon,n}(t). \quad \text{(A23)}$$

Eq. (A23) corresponds to Eq. (8).

In the case of the low bias voltage applied to the leads, the wide band limit (WBL) scheme is expected to be valid, and drastically reduces the computational cost. A Fourier transform of the self-energy due to the lead γ in time domain is defined as

$$\Sigma^{\gamma}(t,t_1) = \frac{1}{2\pi\hbar}\int_{-\infty}^{\infty} \Sigma^{\gamma}(\epsilon)\exp\left(-i\frac{\epsilon}{\hbar}(t-t_1)\right)d\epsilon, \quad \text{(A24)}$$

where $\Sigma^{\gamma}(\epsilon)$ is defined by

$$\Sigma^{\gamma}(\epsilon) = H^{C\gamma}g^{\gamma\gamma}(\epsilon)H^{\gamma C}. \quad \text{(A25)}$$

$g^{\gamma\gamma}(\epsilon)$ is the unperturbed Green's function in energy domain. In the WBL scheme, we impose the approximation as

$$\Sigma^{\gamma}(\epsilon) \approx \Sigma^{\gamma}(\epsilon_F). \quad \text{(A26)}$$

By this approximation, Eq. (A24) becomes

$$\Sigma^{\gamma}(t,t_1) \approx \Sigma^{\gamma}(\epsilon_F)\delta(t-t_1). \quad \text{(A27)}$$

By substituting Eq. (A27) into Eq. (A22), we obtain the equation,

$$\vec{D}_{\pm,\epsilon,n}(t) \approx (\Sigma^{L}(\epsilon_F) + \Sigma^{R}(\epsilon_F))\vec{\Psi}^{C}_{\pm,\epsilon,n}(t). \quad \text{(A28)}$$

APPENDIX B: HOW TO EXTRACT THE MEAN FREE PATH

In this section, we explain the extraction of the mean free path L_m. Figure 6 shows the system length L dependence of the electrical resistance R for an armchair SWNT at 300 K. In the diffusive regime, the L dependence of R is described by

$$R = \frac{R_0}{M}\frac{L}{L_m}, \quad \text{(B1)}$$

where R_0 is the quantum resistance defined by $h/2e^2$, and M is the number of conduction channels ($M = 2$ for an armchair SWNT at the Fermi energy ϵ_F). From Eq. (B1), L_m are extracted as the intersection point of the dotted lines $R = (R_0/2)L/L_m$ and the dash-dotted line $R = R_0/2$ in Fig. 6.

APPENDIX C: HOW TO EXTRACT THE PHASE COHERENCE LENGTH

In this section, we explain the extraction of the phase coherence length L_ϕ. Figure 7 shows the system length L dependence of the coherent component $J_{\epsilon_F}(\omega_F)$ for an armchair SWNT at 300 K. The relation between $J_{\epsilon_F}(\omega_F)$ and L is given by

$$J_{\epsilon_F}(\omega_F) = M\exp\left(-\frac{L}{L_\phi}\right), \quad \text{(C1)}$$

where L_ϕ is the phase coherence length [3] and M is the number of conduction channels ($M = 2$ for an armchair SWNT at the Fermi energy ϵ_F). From Eq. (C1), L_ϕ are extracted as the intersection point of the dotted lines $1 - L/L_\phi$ and the line $J_{\epsilon_F}(\omega_F) = 0$ in Fig. 7.

[1] B. J. van Wees, H. van Houten, C. W. J. Beenakker, J. G. Williamson, L. P. Kouwenhoven, D. van der Marel, and C. T. Foxon, Phys. Rev. Lett. **60**, 848 (1988).

[2] S. Frank, P. Poncharal, Z. L. Wang, and W. A. de Heer, Science **280**, 1744 (1998).

[3] S. Datta, *Electronic Transport in Mesoscopic Systems* (Cambridge University Press, Cambridge, 1995).

[4] Y. Aharonov and D. Bohm, Phys. Rev. **115**, 485 (1959).

[5] P. W. Anderson, Phys. Rev. **109**, 1492 (1958).

[6] A.-P. Jauho, N. S. Wingreen, and Y. Meir, Phys. Rev. B **50**, 5528 (1994).

[7] J. Taylor, H. Guo, and J. Wang, Phys. Rev. B **63**, 245407 (2001).

[8] M. Brandbyge, J.-L. Mozos, P. Ordejon, J. Taylor, and K. Stokbro, Phys. Rev. B **65**, 165401 (2002).

[9] L. Shifren, C. Ringhofer, and D. Ferry, IEEE Trans. Electron Devices **50**, 769 (2003).

[10] D. Querlioz, P. Dollfus, V.-N. Do, A. Bournel, and V. L. Nguyen, J. Comput. Electron. **5**, 443 (2006).

[11] D. Querlioz, J. Saint-Martin, A. Bournel, and P. Dollfus, Phys. Rev. B **78**, 165306 (2008).

[12] X. Zheng, F. Wang, C. Y. Yam, Y. Mo, and G. H. Chen, Phys. Rev. B **75**, 195127 (2007).

[13] H. Ishii, N. Kobayashi, and K. Hirose, Appl. Phys. Express **1**, 123002 (2008).

[14] H. Ishii, S. Roche, N. Kobayashi, and K. Hirose, Phys. Rev. Lett. **104**, 116801 (2010).

[15] H. Ishii, N. Kobayashi, and K. Hirose, Phys. Rev. B **82**, 085435 (2010).

[16] J. R. Hellums and W. R. Frensley, Phys. Rev. B **49**, 2904 (1994).

[17] J. Weston and X. Waintal, J. Comp. Elec. **15**, 1148 (2016).

[18] B. Gaury, J. Weston, M. Santin, M. Houzet, C. Groth, and X. Waintal, Phys. Rep. **534**, 1 (2014).

[19] L. V. Woodcock, Chem. Phys. Lett. **10**, 257 (1971).

[20] J. M. Haile and S. Gupta, J. Chem. Phys. **79**, 3067 (1983).

[21] H. C. Anderson, J. Chem. Phys. **72**, 2384 (1980).

[22] W. A. Harrison, *Electronic Structure and the Properties of Solids: The Physics of the Chemical Bond* (Dover, New York, 1989).

[23] T. Ando, Phys. Rev. B **44**, 8017 (1991).

[24] P. A. Khomyakov, G. Brocks, V. Karpan, M. Zwierzycki, and P. J. Kelly, Phys. Rev. B **72**, 035450 (2005).

[25] As an initial state of $\vec{\Psi}^{\alpha}_{\epsilon_{\mathrm{F}},n}(t)$, we used the steady-state wave function vector obtained from the mode matching method [23,24]. As another way to obtain the initial state, we can use wave function after enough time in the time evolution simulation Eq. (11). For calculating the initial state, the atom positions are fixed at the optimized geometry.

[26] N. Watanabe and M. Tsukada, Phys. Rev. E **62**, 2914 (2000).

[27] N. Hamada, S.-I. Sawada, and A. Oshiyama, Phys. Rev. Lett. **68**, 1579 (1992).

[28] R. Saito, M. Fujita, G. Dresselhaus, and M. S. Dresselhaus, Appl. Phys. Lett. **60**, 2204 (1992).

[29] H.-S. P. Wong and D. Akinwande, *Carbon Nanotube and Graphene Device Physics* (Cambridge University Press, Cambridge, 2011).

[30] J.-Y. Park, S. Rosenblantt, Y. Yaish, V. Sazonova, H. Üstünel, S. Braig, T. A. Arias, P. W. Brouwer, and P. L. McEuen, Nano Lett. **4**, 517 (2004).

[31] L. Lindsay and D. A. Broido, Phys. Rev. B **81**, 205441 (2010).

[32] C. T. White and T. N. Todorov, Nature (London) **393**, 240 (1998).

[33] H. Suzuura and T. Ando, Phys. Rev. B **65**, 235412 (2002).

[34] J. Jiang, R. Saito, Ge. G. Samsonidze, S. G. Chou, A. Jorio, G. Dresselhaus, and M. S. Dresselhaus, Phys. Rev. B **72**, 235408 (2005).